

A Multi-Modality Ovarian Tumor Ultrasound Image Dataset for Unsupervised Cross-Domain Semantic Segmentation

Qi Zhao^{*}, Member, IEEE, Shuchang Lyu^{*}, Graduate Student Member, IEEE, Wenpei Bai^{*}, Linghan Cai^{*}, Binghao Liu, Meijing Wu, Xiubo Sang, Min Yang, Lijiang Chen, Member, IEEE

arXiv:2207.06799v3 [cs.CV] 12 Sep 2022

Abstract—Ovarian cancer is one of the most harmful gynecological diseases. Detecting ovarian tumors in early stage with computer-aided techniques can efficiently decrease the mortality rate. With the improvement of medical treatment standard, ultrasound images are widely applied in clinical treatment. However, recent notable methods mainly focus on single-modality ultrasound ovarian tumor segmentation or recognition, which means there still lacks researches on exploring the representation capability of multi-modality ultrasound ovarian tumor images. To solve this problem, we propose a Multi-Modality Ovarian Tumor Ultrasound (MMOTU) image dataset containing 1469 2d ultrasound images and 170 contrast enhanced ultrasonography (CEUS) images with pixel-wise and global-wise annotations. Based on MMOTU, we mainly focus on unsupervised cross-domain semantic segmentation task. To solve the domain shift problem, we propose a feature alignment based architecture named Dual-Scheme Domain-Selected Network (DS²Net). Specifically, we first design source-encoder and target-encoder to extract two-style features of source and target images. Then, we propose Domain-Distinct Selected Module (DDSM) and Domain-Universal Selected Module (DUSM) to extract the distinct and universal features in two styles (source-style or target-style). Finally, we fuse these two kinds of features and feed them into the source-decoder and target-decoder to generate final predictions. Extensive comparison experiments and analysis on MMOTU image dataset show that DS²Net can boost the segmentation performance for bidirectional cross-domain adaptation of 2d ultrasound and CEUS images. Our proposed dataset and code are all available at https://github.com/cv516Buaa/MMOTU_DS2Net.

Index Terms—Multi-Modality Ultrasound Image Dataset, Cross-Domain Semantic Segmentation, Dual-Scheme Domain-Selected Network, Unsupervised Domain Adaptation, Recognition

^{*} Contribute Equally.

This work was supported by the National Natural Science Foundation of China (grant number 62072021) and the Beijing Hospitals Authority Ascent Plan (grant number DFL20190701) (Primary Corresponding Author: Lijiang Chen. Secondary Corresponding Author: Min Yang).

Qi Zhao, Shuchang Lyu, Linghan Cai, Binghao Liu, Lijiang Chen are with the Department of Electronics and Information Engineering, Beihang University, Beijing, 100191, China, (e-mail: zhaoqi@buaa.edu.cn, lyushuchang@buaa.edu.cn, cailh@buaa.edu.cn, liubinghao@buaa.edu.cn, chenlijiang@buaa.edu.cn).

Wenpei Bai, Meijing Wu, Xiubo Sang, Min Yang are with the Department of Gynecology and Obstetrics, Beijing Shijitan Hospital, Capital Medical University, Beijing, China, (e-mail: baiwp@bjstjth.cn, nancywu0429@foxmail.com, sangxiubo3506@bjstjth.cn, yangmin@bjstjth.cn).

I. INTRODUCTION

OVARIAN cancer is one of the most mortal gynecological diseases. According to recent statistics [1], the ovarian cancer rank 8th among all the gynecological cancers. Diagnosing and detecting ovarian tumors in the early stage can significantly decrease the mortality rate. At present, the commonly used screening techniques are two-dimensional (2d) ultrasound scanning, contrast enhanced ultrasonography (CEUS), Computed Tomography (CT) and Magnetic Resonance Imaging (MRI). Among them, 2d ultrasound scanning is the most widely-applied technique because of more convenience and less impact on human body.

Recently, several methods focus on computer-aided diagnosing and ovarian tumors detection [2]–[6]. Despite their notable works, there still exists the following two main weaknesses. First, recent methods only focus on single-modality images (mainly 2d ultrasound images) segmentation and recognition. There still lacks researches on exploring the representation potential of multi-modality ultrasound images because of lacking standard datasets. Second, even though many notable methods [7]–[11] make huge progress on cross-domain adaptation, there still lacks solution on tackling cross-domain segmentation among multi-modality ultrasound images.

To solve the above-mentioned two weaknesses, we first construct a Multi-Modality Ovarian Tumor Ultrasound (MMOTU) image dataset. MMOTU image dataset consists of two sub-sets with two modalities, which are OTU_2d and OTU_CEUS respectively including 1469 2d ultrasound images and 170 CEUS images. On both of these two sub-sets, we provide pixel-wise semantic annotations and global-wise category annotations. Then, we explore the representation potential of networks on MMOTU image dataset. As shown in Fig.1, we mainly tackle three tasks on MMOTU image dataset. The first task is a semantic segmentation task, which focuses on finding the lesion area of tumor in pixel-wise. The second task is an unsupervised domain adaptation (UDA) based semantic segmentation task, which aims to boost the segmentation performance of target samples only training with source annotated samples. In this paper, we apply segmentation for bidirectional cross-domain adaptation between 2d ultrasound and CEUS images. The third task is a recognition task aiming at classifying the tumor into eight categories. In particular, “Normal ovary” is one of the

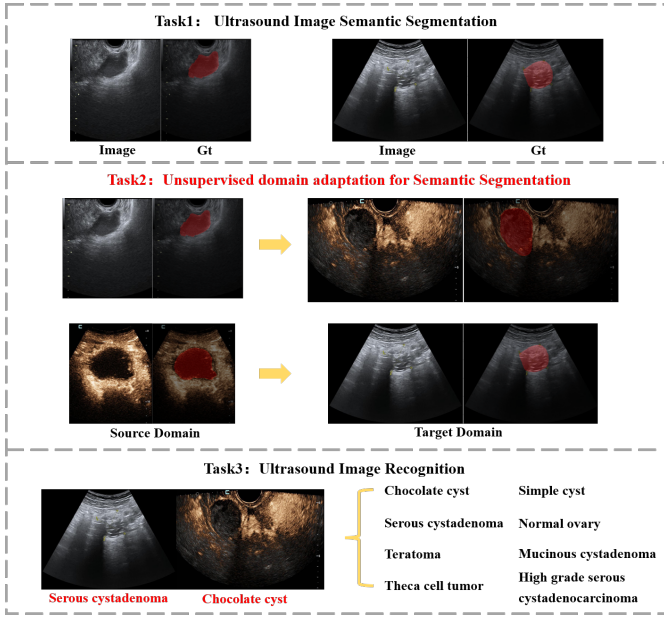


Fig. 1. Task description on MMOTU image dataset. **Task1:** single-modality semantic segmentation. **Task2:** bidirectional unsupervised domain adaptation between OTU_2d and OTU_CEUS for semantic segmentation. **Task3:** single-modality image recognition.

eight categories. In the first and second task, the target region of “Normal ovary” samples is the region of ovary (not the region of tumor).

Recently, deep convolutional neural networks (DCNNs) has shown great success on recognition [2], [12]–[16] and semantic segmentation [17]–[20] of medical images. These two tasks play an important role on computer-aided diagnosis of medical images. Based on MMOTU image dataset, we first tackle single-modality semantic segmentation task. In this paper, we provide four types of notable baseline architectures in semantic segmentation, which are CNN-based “Encoder-Decoder”, transformer-based “Encoder-Decoder”, U-shape networks and spatial-context based two-branch networks.

Based on baseline segmentors, we then tackle the unsupervised domain adaptation based semantic segmentation task. Recent UDA methods solve the domain shift problems mainly by image alignment [10], [11], [21], [22] and feature alignment [7], [23]–[25]. Image alignment based methods apply image translation technique to translate image appearance between domains. Feature alignment utilizes adversarial learning to extract domain-invariant features. In this paper, we propose a feature alignment based method to solve domain shift problems. The motivations to use feature alignment can be summarized in the following three points: (1) Compared to image alignment based methods, feature alignment based methods always require less computation resource in both training and testing phases. (2) Image alignment based methods show strong power when appearance of source and target images have dramatic difference. Intuitively, the main appearance shift between 2d ultrasound and CEUS images is the color (Fig.1), which means this appearance shift problems may not cause heavy feature-shift especially on high-level features. (3) Based

on the baseline segmentors (Fig.1, Task1) trained with source images, we directly apply them on target images and find that the segmentation performance on source-trained model does not decrease dramatically compared to the result on target-trained model. This observation encourages us to explore the potential of feature alignment and distinct/universal feature extraction.

In this paper, our proposed feature alignment based architecture is Dual-Scheme Domain-Selected Network (DS²Net). Specifically, we first design two encoders (E_s and E_t), which map source and target images into two-style features (i.e. E_s will respectively map source and target images into source-style source features and source-style target features. Similarly for E_t). Then, we assume that two-style features of source and target images are not decoupled, which means source-style features may contain some target-style information and vice versa. Based on this assumption, we propose Domain-Distinct-Selected Module (DDSM) to select the distinct feature of each domain. With DDSM, we can decouple the source-style (target-style) features into purer source-style (target-style) features and target-style (source-style) features. Obviously, only decoupling feature into two-style is not reasonable because some information may work on both sides or not work on any side. Therefore, we further propose Domain-Universal-Selected-Module (DUSM) to select the universal features of two domains. With DUSM, we further find the universal information of source/target-style features. Finally, we respectively feed the source-style and target-style features into two decoder-heads (H_s and H_t) for predictions. During optimization, besides supervision from source annotations, we apply adversarial learning to combat the domain shift on the two-style features output from E_s and E_t . This design ensures that two-style features can be aligned into same latent space, making the following feature decoupling easier. To prove the effectiveness of DS²Net, we conduct comparison experiments with recent notable feature alignment based domain adaptation methods [7], [25] on MMOTU image dataset. The encouraging results prove the effectiveness of DS²Net.

In summary, the main contributions are listed as follows:

- We construct a Multi-Modality Ovarian Tumor Ultrasound (MMOTU) image dataset containing 2d ultrasound and CEUS images. For every images in MMOTU image dataset, we provide pixel-wise semantic annotations and global-wise category annotations.
- To the best of our knowledge, we first propose a method (DS²Net) to tackle the cross-domain ovarian tumor segmentation between 2d ultrasound and CEUS images. With this method, we provide an insight on detecting ovarian tumors on multi-modality ultrasound images.
- DS²Net utilizes domain selected modules (DDSM and DUSM) to extract domain-distinct and domain-universal features. Essentially, we provide an insight on using feature decoupling technique to solve domain shift problem.

II. RELATED WORK

A. Computer-Aided Methods on Ovarian Ultrasound Image Datasets

To develop computer-aided methods on medical treatment of ovarian diseases, many methods construct ultrasound image datasets and use DCNNs to tackle the image recognition task. Wu *et al.* [2] construct a 2d-ultrasound image dataset with three types of ovarian tumors (Benign, Borderline and Malignant). This dataset is used for ovarian tumor classification. Followed [2], Wang *et al.* [13] collect annotated samples of serous ovarian tumors (SOTs) and then apply DCNNs to categorize SOTs into Benign, Borderline and Malignant.

Besides recognition task, many notable methods explore the potential of tackling the semantic segmentation task on 2d-ultrasound ovarian images. These methods mainly aim at characterizing the ovarian structure with segmentation techniques. Li *et al.* [6] propose CR-UNet, which integrates the spatial recurrent neural network (RNN) into a plain U-Net to segment the ovary and follicles. Wanderley *et al.* propose fCNN [26] to automatically characterize ovarian structures. Both CR-UNet and fCNN are trained on their own collected 2d-ultrasound ovarian image datasets with pixel-wise annotations of ovary and follicles. Recently, several advanced methods are proposed to characterize the ovarian structure through directly processing 3d-ultrasound ovarian volumes. Mathur *et al.* propose S-Net [27] to simultaneously segment ovary and follicles in 3d-ultrasound volumes. Yang *et al.* [4] propose C-Rend (contrastive rendering) on ovary and follicles segmentation and further apply it into a semi-supervised learning framework. Both S-Net and C-Rend are trained on their own collected 3d-ultrasound ovarian volume datasets.

B. Semantic Segmentation on Medical Images

Semantic segmentation has become an important medical image processing technique, which is widely applied in many practical applications, such as organ structure characterization, lesion area detection and cell segmentation. In this field, U-Net [17] is one of the most famous methods, which creates short-cuts between encoder and decoder to capture contextual and precise localization information. Followed U-Net, U-Net++ [19] connects encoder and decoder using a series of nested dense convolutional blocks. Compared to U-Net, this design can further bridge the semantic gap between feature maps from encoder and decoder. In recent years, attention mechanism substantially promotes semantic segmentation. Oktay *et al.* [28] propose an attention U-Net. Before fusing the feature maps from encoder and decoder, attention U-Net inserts an attention gate to control the spatial-wise feature importance. Besides applying spatial-wise attention mechanism, Chen *et al.* [29] propose FED-Net, which uses a channel-wise attention mechanism to improve the performance of liver lesion segmentation. There are also many notable works [30]–[32] aiming at mixing spatial-wise and channel-wise attention mechanisms.

Transformer is a cutting-edge structure utilizing self-attention mechanism to capture important region of images. On medical image semantic segmentation, TransFuse [20] and TransUNet [18] both employ ViT (Vision Transformer) [33] as

TABLE I
THE DATA DISTRIBUTION OF MMOTU IMAGE DATASET.

Data type	Training set	Testing set	category number
OTU_2d	1000	469	8
OTU_CEUS	70	100	8

encoder for feature extraction. Swin-UNet [34] applies Swin-Transformer [35] on both encoder and decoder to explore the learning potential on long-range semantic information. SegTran [36] further proposes a squeeze-and-expansion transformer for more diversified representations.

C. Unsupervised Domain Adaptation on Medical Images

UDA mainly aims to alleviate the domain shift problem when applying a source-trained model on target domain data. There are mainly two types of methods on UDA based semantic segmentation task, which are image alignment and feature alignment based methods. Image alignment based methods always adopt image translation [9], [37] to align image appearance between source and target domain. Chen *et al.* [10] and Ouyang *et al.* [21] propose a generator for source-to-target transformation and then optimize the segmentor by the target-style source image with corresponding annotations. Zou *et al.* [11] and Zeng *et al.* [22] further add a target-to-source generator besides source-to-target generator to bridge source and target domain with a balanced flow. Feature alignment based methods solve the domain shift problem through exploring domain invariant features. Zeng *et al.* [25] propose feature and entropy map discriminators to explore the representation potential of domain invariant features. Wang *et al.* [24] propose pOSAL to segment the optic disc and optic cup from different fundus image datasets in a joint manner. pOSAL exploits UDA with feature alignment mechanism to ease the domain shift. Moreover, some other notable feature alignment based methods, such as AdapSegNet [7] and SSF-DAN [23] both achieve great success on both natural scene images and medical images.

III. DATASET

A. Establishment

To tackle the cross-domain ovarian tumor segmentation task, we first propose MMOTU image dataset. All images are obtained from Beijing Shijitan Hospital, Capital Medical University. Our dataset contains 1639 ovarian ultrasound images collected from 294 patients. As shown in Tab.I, MMOTU image dataset contains two sub-sets with two modalities, where OTU_2d and OTU_CEUS respectively consist of 1469 2d ultrasound images and 170 CEUS images. On two sub-sets, we split them into training and testing sets. It is worth noting that, testing set contains more images than training set in OTU_CEUS, because we hope to first guarantee the evaluation quality. When we tackle cross-domain segmentation, more testing images will make the results more convincing. Since

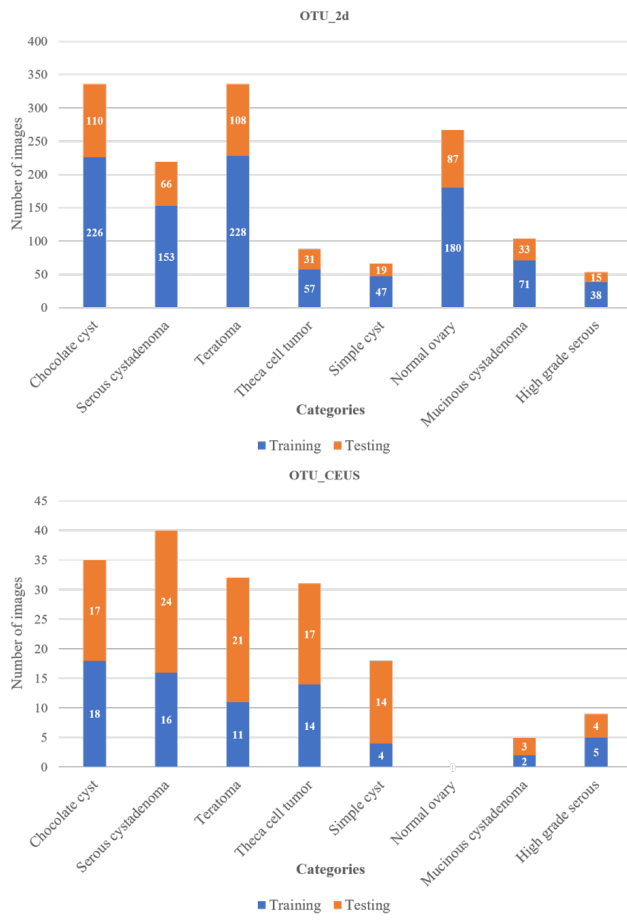


Fig. 2. The number of samples containing in each category.

we are continually collecting CEUS images, so more samples will be soon added in the training set.

MMOTU image dataset has eight typical categories of ovarian tumor (Fig.1). Fig.2 further shows the sample distribution of each category in detail. From Fig.2, we find the following two points. (1) Samples of each category are unbalanced. This is mainly because some types tumors are more common while some types of tumors are rarer. (2) In OTU_CEUS, some categories only contain few-shot samples, which is easy to cause underfitting. Even though we can not provide more samples for those few-shot categories, it is a chance for researchers to explore the potential on few-shot ovarian tumor segmentation or classification. We will also continually collecting CEUS images and extending our OTU_CEUS in the future. (3) “Normal Ovary” category has no samples in OTU_CEUS, because CEUS technology is usually a further examination after 2d ultrasound examination, which is mainly applied to confirm the tumor types (e.g. Benign, Borderline, Malignant or our proposed specific types). It means the CEUS images hardly have “Normal Ovary” category. Under this situation, the segmentation and recognition tasks on OTU_CEUS become seven-category tasks (not eight-category). When tackling UDA segmentation task, no matter OTU_2d is served as source or target set, we will remove the “Normal Ovary” samples from OTU_2d to make the experiments reasonable. In other

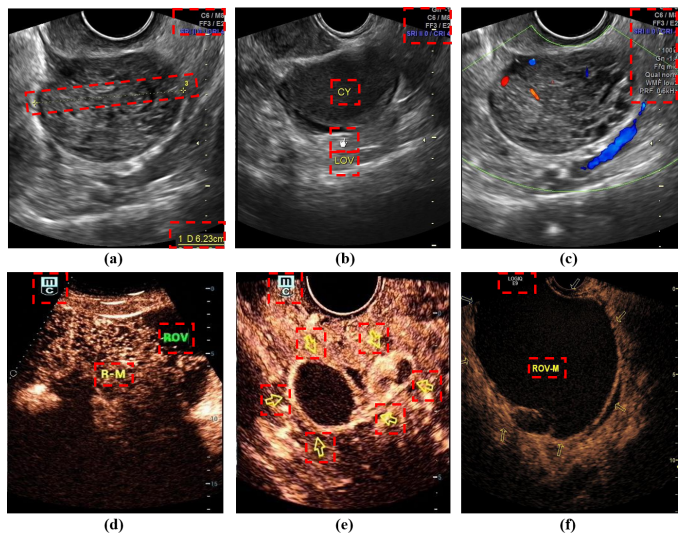


Fig. 3. Typical samples in MMOTU image dataset. Images in first and second row are respectively 2d ultrasound and CEUS image samples.

words, UDA segmentation task is also a seven-category task. (4) The segmentation and recognition tasks on OTU_2d are eight-category task including “Normal Ovary” category.

For almost every images, only one type of tumor appears. Therefore, we transform an seven/eight-category segmentation task into binary lesion area segmentation task (Task1 and Task2) and tumor recognition task (Task3).

On MMOTU image dataset, the pixel-wise semantic annotation and global-wise category annotation are provided by 27 experts of Obstetrics and Gynecology department. Each image is first annotated by one expert and then checked by another one expert, which guarantees the annotating quality. During annotating, experts refer to pathological reports, which makes the annotations accurate and convincing.

B. Data Analysis

In MMOTU image dataset, all images have been analyzed by experts using specialized software, so some symbols like “lines” (Fig.3(a)), “hands” (Fig.3(b)), “characters” (Fig.3(d) and Fig.3(f)) or “arrows” (Fig.3(e)) are marked by them on images. When we collect the images, most of them contain those symbols. Fig.3 shows some typical samples. Particularly, OTU_2d sub-set contains 216 Color Doppler Flow Images (CDFI), where the rest 1253 images are traditional 2d ultrasound images; The images in OTU_CEUS sub-set are extracted from CEUS sequences. When collecting the images, we find that all images contain the private information of patients. According to privacy policy, we manually crop the images to remove the private information of patients and make sure that the published MMOTU image dataset will not contain any private information.

Images in dataset have different scales. Fig.4 shows the distribution of image scale. In OTU_2d, the width and height of images respectively range from 302~1135 and 226~794 pixels. In OTU_CEUS, the width and height of images respectively range from 330~888 and 218~657 pixels. Before

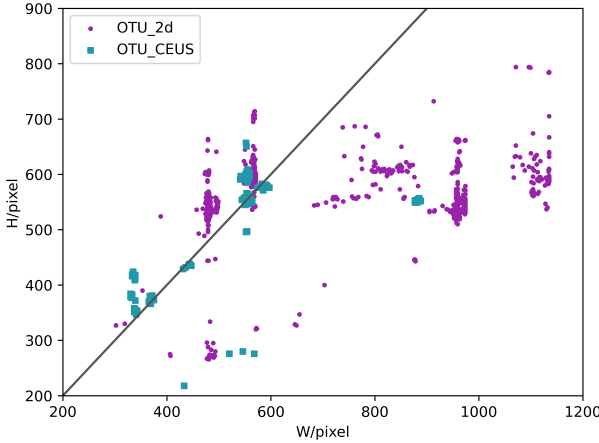


Fig. 4. The scatter plot showing the distribution of image scale.

TABLE II

COMPARISON BETWEEN MMOTU IMAGE DATASET AND OTHER OVARIAN ULTRASOUND IMAGE DATASET. HERE, "VOL" INDICATES VOLUMES.

Methods	Data Number	Category Number	Data Type (2d/3d/CEUS)	Task (Cls/Seg/DA-Seg)
Wu et al. [2]	988	3	✓/✗/✗	✓/✗/✗
Wang et al. [13]	412	3	✓/✗/✗	✓/✗/✗
Wanderley et al. [26]	87	3	✓/✗/✗	✗/✓/✗
Li et al. [6]	3204	3	✓/✗/✗	✗/✓/✗
Narra et al. [38]	105 (vol)	3	✓/✓/✗	✗/✓/✗
Mathur et al. [27]	66 (vol)	3	✓/✓/✗	✗/✓/✗
Yang et al. [4]	307 (vol)	3	✓/✓/✗	✗/✓/✗
Ours	1639	8	✓/✗/✓	✓/✓/✓

training, input images will be randomly resized and cropped to 384×384 .

Tab.II shows the comparison between MMOTU image dataset and previous ovarian ultrasound image datasets. From the comparison, we make analysis in the following points. First, [2], [13] construct ovarian 2d ultrasound datasets to train a model which can categorize the ovarian tumor into Benign, Borderline and Malignant. Comparing with their methods, our dataset contains eight concrete ovarian tumor categories (Fig.1). Second, [4], [6], [26], [27], [38] construct ovarian 2d or 3d ultrasound datasets for ovarian structure segmentation. [6], [26] fill their dataset only with 2d ultrasound slices and [4], [27], [38] fill their dataset with both 2d ultrasound slices and 3d ultrasound volumes. Strictly speaking, 2d ultrasound slices and 3d ultrasound volumes belong to single-modality data, because every 2d ultrasound slices are extracted from a specific 3d ultrasound volume. Comparing with their datasets, our dataset contains 2d ultrasound slices together with CEUS images, which is a typical multi-modality dataset. Generally speaking, we construct a multi-modality ovarian tumor ultrasound dataset to tackle multi-tasks including tumor classification, lesion area segmentation and unsupervised cross-domain

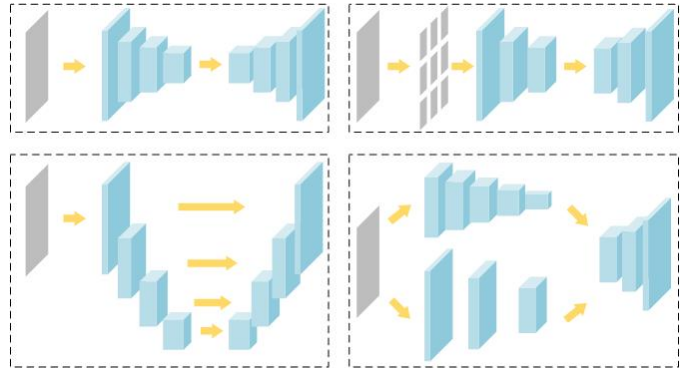


Fig. 5. The diagram of recent notable architectures on semantic segmentation. **top-left:** CNN-based "Encoder-Decoder", **top-right:** Transformer-based "Encoder-Decoder", **bottom-left:** U-shape networks, **bottom-right:** Spatial-context based two-branch networks.

segmentation. Moreover, our dataset provides an insight on applying DCNNs to deal with CEUS images.

IV. PROPOSED METHOD

A. Single-Modality Image Segmentation/Recognition

Based on MMOTU image dataset, we first tackle single-modality semantic segmentation task (Fig.1 Task1) to provide series of baseline segmentors. Fig.5 shows the diagrams of four notable architectures in semantic segmentation. For CNN-based "Encoder-Decoder", we select two notable segmentors, PSPNet [39] and DANet [40]. The former utilizes the spatial-wise contextual information, the latter introduces spatial-wise and channel-wise attention information in segmentors. Transformer-based "Encoder-Decoder" is a series of cutting-edge architectures integrating transformers into segmentors to enhance the performance with self-attention mechanism. In this paper, we reimplement SegFormer [41], which is an efficient and lightweight yet powerful semantic segmentation architecture. U-shape networks are most common-used on medical image segmentation. In this paper, we provide two novel segmentors, which are U-Net [17] and TransUNet [18]. As another innovative series of segmentors, spatial-context based two-branch networks use spatial-branch with wide channels and shallow layers and context-branch to respectively capture low-level high-resolution features and high-level context features. Here, we reimplement BiseNetV2 [42] as representative of this type of segmentors.

Besides segmentation task, we also tackle single-modality image recognition task (Fig.1 Task3) on MMOTU image dataset. Same as Task1, we provide series of baseline classification models, which are classical and high-efficiency models, ResNet [43], DenseNet [44] and EfficientNet [45].

B. Unsupervised Domain Adaptation for Semantic Segmentation

In this paper, exploiting the potential of lesion area segmentation for bidirectional UDA between 2d ultrasound and CEUS images is our main focus. To solve the domain shift problem, we propose a feature alignment based method, DS²Net. The overview of the architecture is shown in Fig.6.

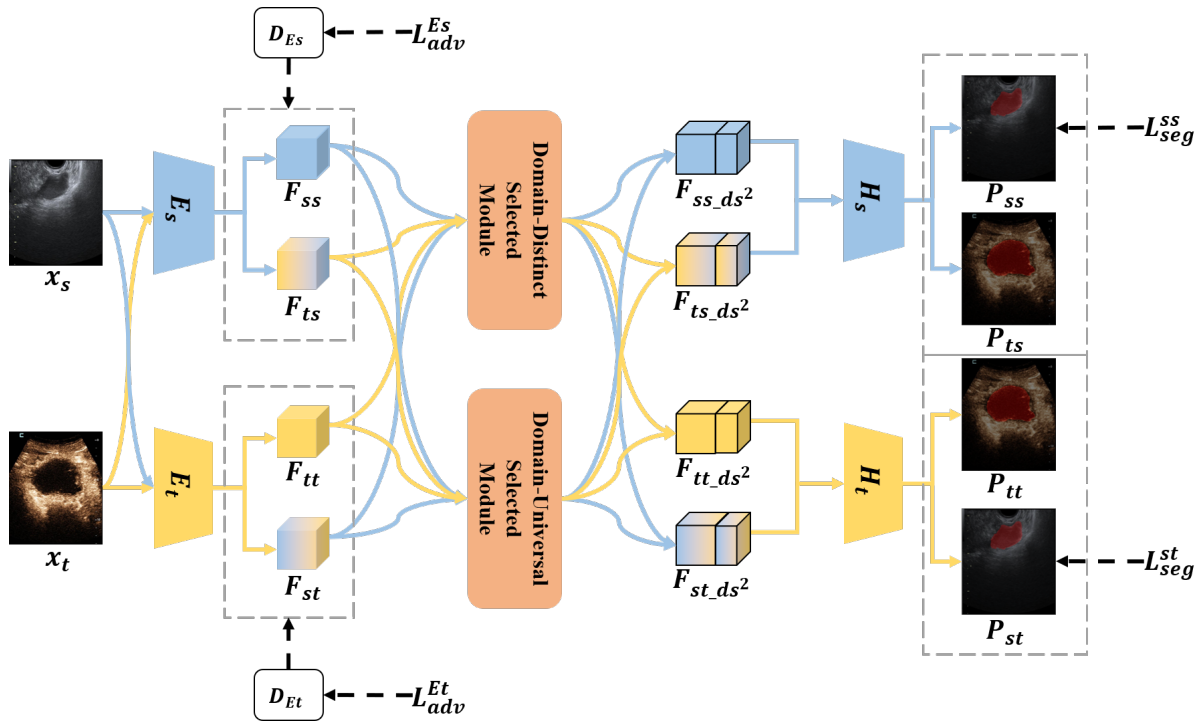


Fig. 6. The architecture of DS²Net. Source and target images are first fed into E_s and E_t and the output feature maps are respectively $\{F_{ss}, F_{st}\}$ and $\{F_{tt}, F_{ts}\}$. Then, domain distinct selected module (DDSM) and domain universal selected module (DUSM) are applied on $\{F_{ss}, F_{st}\}$ and $\{F_{tt}, F_{ts}\}$. After processing by DDSM and DUSM, the domain selected features ($\{F_{ss_ds^2}, F_{st_ds^2}\}$; $\{F_{tt_ds^2}, F_{ts_ds^2}\}$) pass through H_s and H_t to generate final predictions. During optimization, we apply symmetric adversarial loss ($\mathcal{L}_{E_s}^{adv}, \mathcal{L}_{E_t}^{adv}$) and segmentation loss ($\mathcal{L}_{seg}^{ss}, \mathcal{L}_{seg}^{st}$). Specifically, the discriminators $\{D_{E_s}, D_{E_t}\}$ are designed for feature alignment. During inference, we apply ensemble strategy to integrate the two predictions of target images ($\{P_{tt}, P_{ts}\}$).

1) Adversarial Learning for Feature Alignment: As shown in Fig.6, we respectively design E_s and E_t for feature extraction of source and target images. Obviously, we hope that both E_s and E_t have the general representation capability on source and target images. Therefore, we apply adversarial learning on E_s and E_t to alleviate the representation gap caused by domain shift. Eq.1 ~ Eq.4 show this process.

$$\begin{aligned} \mathcal{L}_{adv}^{E_s}(E_s, D_{E_s}) &= \mathbb{E}_{x_s \sim X_s} [\log(D_{E_s}(F_{ss}))] \\ &+ \mathbb{E}_{x_t \sim X_t} [\log(1 - D_{E_s}(F_{ts}))] \end{aligned} \quad (1)$$

$$F_{ss} = E_s(x_s), \quad F_{ts} = E_s(x_t) \quad (2)$$

$$\begin{aligned} \mathcal{L}_{adv}^{E_t}(E_t, D_{E_t}) &= \mathbb{E}_{x_t \sim X_t} [\log(D_{E_t}(F_{tt}))] \\ &+ \mathbb{E}_{x_s \sim X_s} [\log(1 - D_{E_t}(F_{st}))] \end{aligned} \quad (3)$$

$$F_{tt} = E_t(x_t), \quad F_{st} = E_t(x_s) \quad (4)$$

Here, x_s and x_t respectively denote source and target images. D_{E_s} and D_{E_t} are two discriminators. $F_{ss}, F_{ts}, F_{tt}, F_{st}$ are respectively denoted as source-style source feature, source-style target feature, target-style target feature and target-style source feature. We adopt min-max criterion to optimize E_s and E_t , which can be described as $\min_{E_s} \max_{D_{E_s}} \mathcal{L}_{adv}^{E_s}(E_s, D_{E_s})$ and $\min_{E_t} \max_{D_{E_t}} \mathcal{L}_{adv}^{E_t}(E_t, D_{E_t})$. With this feature alignment on E_s and E_t , two encoders have better ability to represent images from two domains. Furthermore, two encoders can provide one more feature map for image from each domain, which enriches the representations.

2) Domain Distinct & Domain Universal Selected Modules:

As shown in Eq.2 and Eq.4, we design two encoders to extract source-style and target-style features for source and target images. Based on the observation that directly applying a source-trained segmentation model on target images will not cause dramatic performance decrease, we make the following assumptions. (1) Between 2d ultrasound and CEUS images, there may exist some easy-extracted universal features, which have positive influence on segmenting images from both these two domains. (2) Since there still exists some performance gap when simply evaluating target images on source-trained models, we believe that domain distinct features also exist. (3) Distinct and universal features can be decoupled from source-style and target-style features. Instructed by the above assumptions, we design Domain Distinct Selected Modules (DDSM) and Domain Universal Selected Modules (DUSM).

DDSM: As shown in Fig.6, source and target images are both represented as source-style and target-style features, which respectively are $\{F_{ss}, F_{st}\}$ ($\mathbb{R}^{C \times H \times W}$) and $\{F_{tt}, F_{ts}\}$ ($\mathbb{R}^{C \times H \times W}$). After applying adversarial learning, E_s and E_t can better represent two domain images as source-style and target-style features. To further extract purer feature specifically for each domain, we propose DDSM.

As shown in Fig.7, we first fuse source-style and target-style features. Then, we apply global average pooling and a dimension-reduction fully-connected layer ($f(\cdot)$) to generate a global-wise fused prototype ($z_{st_sty} \in \mathbb{R}^{C' \times 1 \times 1}$). We

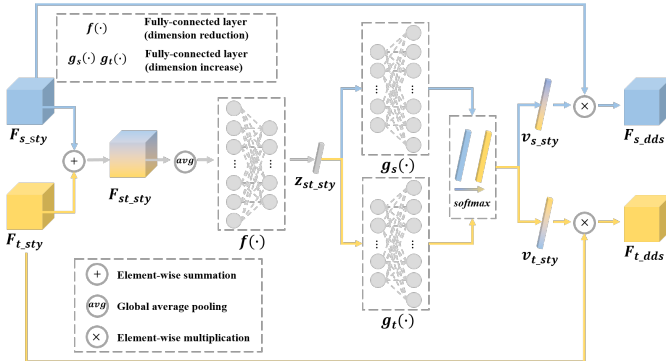


Fig. 7. The architecture of domain-distinct selected module. Here, $\{F_{s_sty}, F_{t_sty}\}$ are respectively source-style and target-style features of source or target images ($\{F_{ss}, F_{st}\}$ or $\{F_{tt}, F_{ts}\}$). Two-style features are first integrated to generate a fused prototype (Z_{st_sty}). Then, we adopt channel-wise attention to obtain channel-wise weighted vectors ($\{v_{s_sty}, v_{t_sty}\}$) for F_{s_sty} and F_{t_sty} . Finally, we multiply $\{v_{s_sty}, v_{t_sty}\}$ on F_{s_sty} and F_{t_sty} in channel-wise to obtain domain distinct features ($\{F_{s_dds}, F_{t_dds}\}$).

formulate this process in Eq.5.

$$\begin{aligned} z_{st_sty} &= f\left(\frac{1}{HW} \sum_{h=1}^H \sum_{w=1}^W (F_{st_sty}(h, w))\right) \\ &= f\left(\frac{1}{HW} \sum_{h=1}^H \sum_{w=1}^W (F_{s_sty}(h, w) + F_{t_sty}(h, w))\right) \end{aligned} \quad (5)$$

Then, we serve z_{st_sty} as guidance to create channel-wise weighted vectors (v_{s_sty} and $v_{t_sty} \in \mathbb{R}^{C \times 1 \times 1}$) using *softmax* operation. Eq.6 and Eq.7 show this operation, where $g_s(\cdot)$ and $g_t(\cdot)$ are dimension-increase fully-connected layers.

$$v_{s_sty} = \frac{e^{g_s(z_{st_sty})}}{e^{g_s(z_{st_sty})} + e^{g_t(z_{st_sty})}} \quad (6)$$

$$v_{t_sty} = \frac{e^{g_t(z_{st_sty})}}{e^{g_s(z_{st_sty})} + e^{g_t(z_{st_sty})}} \quad (7)$$

Finally, the final domain distinct selected features (F_{s_dds} and $F_{t_dds} \in \mathbb{R}^{C \times H \times W}$) are calculated through channel-wise multiplication shown in Eq.8.

$$F_{s_dds} = F_{s_sty} \times v_{s_sty}, \quad F_{t_dds} = F_{t_sty} \times v_{t_sty} \quad (8)$$

From Eq.6 to Eq.7, we find that $v_{s_sty} + v_{t_sty} = 1$, which means we force the source-style and target-style features to have complementary channel combinations. With this design, “source-style features are more source-style while target-style features are more target-style”.

DUSM: With DDSM, we obtain purer source-style and target-style features, but it may overlook the universal features benefiting both source and target images. Therefore, we further design DUSM to extract universal features of F_{s_sty} and F_{t_sty} . As shown in Fig.8, we first fuse source-style and target-style features similar to DDSM (Eq.9).

$$\begin{aligned} Z_{st_sty} &= f_c\left(\frac{1}{HW} \sum_{h=1}^H \sum_{w=1}^W (F_{st_sty}(h, w))\right) \\ &= f_c\left(\frac{1}{HW} \sum_{h=1}^H \sum_{w=1}^W (F_{s_sty}(h, w) + F_{t_sty}(h, w))\right) \end{aligned} \quad (9)$$

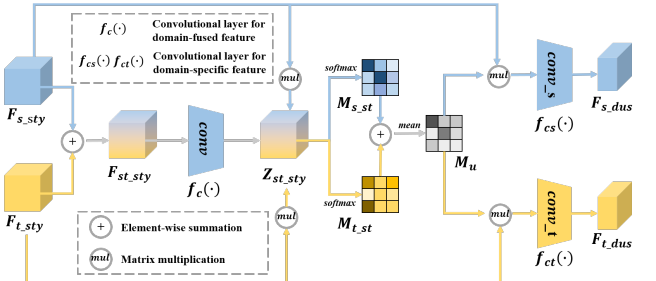


Fig. 8. The architecture of domain-universal selected module. Two-style features are first integrated to generate a fused feature (Z_{st_sty}). Then, we adopt matrix multiplication operation to obtain attention masks ($\{M_{s_sty}, M_{t_sty}\}$) for F_{s_sty} and F_{t_sty} . Next, we average M_{s_sty} and M_{t_sty} for a universal attention mask (M_u). Finally, we serve M_u as universal guidance on F_{s_sty} and F_{t_sty} to obtain domain universal features ($\{F_{s_dus}, F_{t_dus}\}$).

Here, $Z_{st_sty} (\mathbb{R}^{C \times H \times W})$ represent domain fused feature. We then perform matrix multiplication between Z_{st_sty} and $\{F_{s_sty}, F_{t_sty}\}$. The output attention masks ($\{M_{s_sty}, M_{t_sty}\} \in \mathbb{R}^{C \times C}$) are averaged for universal attention mask ($M_u \in \mathbb{R}^{C \times C}$). This process is shown in Eq.10 ~ Eq.12.

$$M_{s_sty}(j, i) = \frac{e^{F_{s_sty}(i) \cdot Z_{st_sty}(j)}}{\sum_{i=1}^C (e^{F_{s_sty}(i) \cdot Z_{st_sty}(j)})} \quad (10)$$

$$M_{t_sty}(j, i) = \frac{e^{F_{t_sty}(i) \cdot Z_{st_sty}(j)}}{\sum_{i=1}^C (e^{F_{t_sty}(i) \cdot Z_{st_sty}(j)})} \quad (11)$$

$$M_u(j, i) = \frac{M_{s_sty}(j, i) + M_{t_sty}(j, i)}{2} \quad (12)$$

where F_{s_sty} , F_{t_sty} and Z_{st_sty} are reshaped to $\mathbb{R}^{C \times (HW)}$. “(j, i)” indicates the impact measurement between i^{th} channel of $\{F_{s_sty}, F_{t_sty}\}$ and j^{th} channel of Z_{st_sty} .

Finally, we use M_u to extract the universal feature from F_{s_sty} and F_{t_sty} , which are F_{s_dus} and $F_{t_dus} (\mathbb{R}^{C'' \times H \times W})$. This formulation is shown in Eq.13.

$$F_{s_dus} = f_{cs}(M_u * F_{s_sty}), \quad F_{t_dus} = f_{ct}(M_u * F_{t_sty}) \quad (13)$$

In summary, we extract the universal feature by finding M_u , which measures the joint impact between source/target-style features and domain fused feature. The larger element in M_u indicates that one channel of fused domain features have high impact both on same channel of source-style and target-style features. Essentially, we utilize a domain universal attention mask to select the universal features in channel-wise.

3) Optimization: In this paper, we apply segmentation loss and adversarial loss to jointly optimize the DS²Net. As for segmentation loss, We apply cross-entropy loss, which can be formulated as Eq.14.

$$\begin{aligned} \mathcal{L}_{seg}(E_s, H_s, E_t, H_t) &= \mathcal{L}_{seg}^{ss}(E_s, H_s) + \mathcal{L}_{seg}^{st}(E_t, H_t) \\ &= \mathbb{E}_{x^s \sim X^s} [-y_s \log(H_s(F_{ss_ds}^2))] \\ &\quad + \mathbb{E}_{x^s \sim X^s} [-y_s \log(H_t(F_{st_ds}^2))] \end{aligned} \quad (14)$$

TABLE III

IMPLEMENTATION DETAILS OF SINGLE-MODALITY SEMANTIC SEGMENTATION. “ \dagger ” MEANS LOADING IMAGENET-PRETRAINED WEIGHTS [46]. “RES50”, “MIT_B5” “ViT” RESPECTIVELY DENOTE RESNET-50 [43], MIX TRANSFORMER [41] AND VISION TRANSFORMER [33].

Methods	Optimizer	Initial LR	LR Decay	Backbone	Iterations
PSPNet	SGD	0.01	poly	Res50 \dagger	20k
DANet	SGD	0.01	poly	Res50 \dagger	20k
SegFormer	Adam	0.00006	poly	mit_b5 \dagger	80k
U-Net	SGD	0.01	poly	U-Net \dagger	80k
TransUNet	SGD	0.01	poly	Res50+ViT \dagger	80k
BiseNetV2	SGD	0.05	poly	BiseNetV2 \dagger	80k

where H_s and H_t are two decoder-heads respectively for source-style and target-style features. $\mathbf{F}_{ss.ds^2} = \text{cat}(\mathbf{F}_{ss.ds}, \mathbf{F}_{ss.dus})$; $\mathbf{F}_{st.ds^2} = \text{cat}(\mathbf{F}_{st.ds}, \mathbf{F}_{st.dus})$. “cat” denotes concatenation. As shown in Eq.8, Eq.13, $\{\mathbf{F}_{ss.ds^2}, \mathbf{F}_{st.ds^2}\} \in \mathbb{R}^{(C+C') \times H \times W}$.

To optimize the whole architecture, we apply combined loss (\mathcal{L}) shown in Eq.15. $\{\lambda_{adv}^{E_s}, \lambda_{adv}^{E_t}\}$ are trade-off hyper-parameters adjusting the impact of each loss item.

$$\begin{aligned} \mathcal{L} = & \mathcal{L}_{seg}(E_s, H_s, E_t, H_t) \\ & + \lambda_{adv}^{E_s} \mathcal{L}_{adv}^{E_s}(E_s, D_{E_s}) + \lambda_{adv}^{E_t} \mathcal{L}_{adv}^{E_t}(E_t, D_{E_t}) \end{aligned} \quad (15)$$

From the perspective of backward optimization process, we find the following points. (1) Through adversarial learning, E_s and E_t have the basic representation ability on source and target images avoiding representation distortion on target images. (2) Based on adversarial learning and DDSM/DUSM, the segmentation loss ($\mathcal{L}_{seg}^{ss}(E_s, H_s)$ and $\mathcal{L}_{seg}^{st}(E_t, H_t)$) can force $\{E_s, H_s\}$ and $\{E_t, H_t\}$ to have specific representation trend (e.g. $\{E_t, H_t\}$ tends to represent source and target images into target style). Optimized like this, the whole architecture becomes more friendly to target image.

V. EXPERIMENTS AND ANALYSIS

A. Single-Modality Semantic Segmentation Results

1) *Implementation Details*.: As mentioned in Sec.IV Subsec.A and Fig.5, we reimplement the six baseline segmentors on MMOTU image dataset. Before training, input images are randomly resized and cropped to 384×384 . A series of data augmentation methods, such as “RandomFlip” are applied. Towards the four types of segmentors, the implementation details are shown in Tab.III. Here, when optimizer is SGD, the momentum is set as 0.9 and the weight decay value is 0.0005. When optimizer is Adam, the weight decay value is 0.01. All segmentors adopt “poly” to adjust learning rate, where the final learning rate will be divided by 100 times and the power is set to 0.9.

2) *Single-Modality Semantic Segmentation Experiments*.: The single-modality segmentation results are shown in Tab.IV. The IoU value indicates the intersection of union between predicted and annotated lesion area. The $mIoU$ value indicates the average IoU value of lesion area and background. From

TABLE IV

SINGLE-MODALITY SEGMENTATION RESULTS ON MMOTU IMAGE DATASET. WE ADOPT IoU (INTERSECTION OVER UNION) AS METRIC.

Methods	OTU_2d		OTU_CEUS	
	$IoU(\%)$	$mIoU(\%)$	$IoU(\%)$	$mIoU(\%)$
PSPNet	82.01	89.41	71.01	81.6
DANet	82.2	89.53	70.3	81.43
SegFormer	82.46	89.88	73.03	83.0
U-Net	79.91	86.80	69.18	80.04
TransUNet	81.31	89.01	70.15	80.82
BiseNetV2	79.37	86.13	70.25	80.98

TABLE V

TRAINING DETAILS OF CROSS-DOMAIN SEMANTIC SEGMENTATION. DS^2Net_P AND DS^2Net_T RESPECTIVELY DENOTE THE DS^2Net FOLLOWING PSPNET AND SEGFORMER.

Methods	Encoders/DDSM/DUSM		Decoder-Heads		Discriminator	
	optimizer	initial (LR)	optimizer	initial (LR)	optimizer	initial (LR)
DS^2Net_P	SGD	0.01	SGD	0.02	Adam	0.00025
DS^2Net_T	Adam	0.00006	Adam	0.00001	Adam	0.00001

Tab.IV, we observe that U-Net and BiseNetV2 show poorer performance compared to other methods. SegFormer outperforms other methods on OTU_2d and OTU_CEUS. Especially on OTU_CEUS, which has less training samples, SegFormer performs even stronger.

B. Cross-Domain Semantic Segmentation Results

1) *Implementation Details*.: As shown in Fig.6, our proposed DS^2Net is a symmetric “Encoder-Decoder” architecture. Therefore, we follow PSPNet and SegFormer to design DS^2Net . Specifically, when following PSPNet, we adopt ResNet-50 as encoders (E_s, E_t) and adopt “PSPHead” as decoder-heads (H_s, H_t). When following SegFormer, we adopt “Hierarchical Transformer” as encoders and adopt “All-MLP” as decoder-heads. For the two discriminators ($\{D_{E_s}, D_{E_t}\}$), we follow the common-applied configuration of PatchGAN [37]. $\{D_{E_s}, D_{E_t}\}$ consist of 4 convolutional layers with kernels as size of 4×4 . The stride of the first two layers is 2 while the the last two layers set the stride as 1. The output channels of each layer are $\{64, 128, 256, 1\}$. Different from previous methods, we remove the instance normalization and only leave a leaky ReLU after each convolutional layer. The training details are shown in Tab.V. Additionally, we select binary cross entropy loss as adversarial loss function and the training factors ($\{\lambda_{adv}^{E_s}, \lambda_{adv}^{E_t}\}$) are set as 0.005.

2) *No Domain Adaptation Experiments*.: Before evaluating the domain adaptation performance of DS^2Net on MMOTU image dataset, we first conduct no domain adaptation experiment, which directly applies a source-trained model on target images. The results are shown in Tab.VI. Previous methods [10], [11] apply no domain adaptation experiment between CT and MRI images. The segmentation results always dramatically decrease (40~60% lower than single-modality training).

TABLE VI

COMPARISON BETWEEN SINGLE-MODALITY SEGMENTATION AND NO DOMAIN ADAPTATION (w/o DA) SEGMENTATION. THE LEFT AND RIGHT OF \rightarrow INDICATE SOURCE AND TARGET DATASET RESPECTIVELY.
RESULTS OF PSPNET AND SEGFORMER ARE OBTAINED BY TRAINING AND EVALUATING ON SINGLE-MODALITY TARGET DATASET.

Methods	OTU_CEUS \rightarrow OTU_2d		OTU_2d \rightarrow OTU_CEUS	
	<i>IoU</i> (%)	<i>mIoU</i> (%)	<i>IoU</i> (%)	<i>mIoU</i> (%)
PSPNet	82.01	89.41	71.01	81.6
PSPNet (w/o DA)	44.54	67.52	50.57	67.87
SegFormer	82.46	89.88	73.03	83.0
SegFormer (w/o DA)	56.28	74.04	61.11	75.45

TABLE VII

COMPARISON WITH PREVIOUS NOTABLE FEATURE ALIGNMENT BASED UDA METHOD FOR OVARIAN LESION AREA SEMANTIC SEGMENTATION.

Methods	OTU_CEUS \rightarrow OTU_2d		OTU_2d \rightarrow OTU_CEUS	
	<i>IoU</i> (%)	<i>mIoU</i> (%)	<i>IoU</i> (%)	<i>mIoU</i> (%)
PSPNet (w/o DA)	44.54	67.52	50.57	67.87
AdapSegNet_P	49.77	69.25	56.14	71.8
EGUDA_P	51.56	70.45	58.42	73.98
DS ² Net_P (ours)	54.06	71.87	61.85	75.75
SegFormer (w/o DA)	56.28	74.04	61.11	75.45
AdapSegNet_T	63.79	77.89	65.52	78.27
EGUDA_T	59.39	75.48	62.11	76.3
DS ² Net_T (ours)	65.42	79.2	69.81	80.86

Compared to previous results, our results on domain adaptation do not decrease by large margin, E.g. when SegFormer is trained with OTU_2d and evaluated on OTU_CEUS, the *IoU* value decreases by 11.92% (73.03% \sim 61.11%) comparing with target-trained SegFormer. It worth noting that the results training with OTU_2d and evaluating on OTU_CEUS are more valuable, because OTU_2d has more training samples than OTU_CEUS (Tab.I). No domain adaptation experiments results inspires us to explore the potential of feature alignment and distinct/universal feature extraction.

3) Cross-Domain Semantic Segmentation Experiments.: To prove the effectiveness of DS²Net, we reimplement two notable feature-alignment based method, which are AdapSegNet [7] and EGUDA [25] on MMOTU image dataset. For fairly comparison, minor modifications are applied. For AdapSegNet and EGUDA, we respectively replace the original shared segmentation network and segmentor with PSPNet or SegFormer. For the discriminator, we adopt the same PatchGAN as $\{D_{E_s}, D_{E_t}\}$ of DS²Net. Tab.VII shows the comparison results. Obviously, our proposed DS²Net perform much stronger than AdapSegNet and EGUDA. Particularly, when adapting OTU_2d to OTU_CEUS, the lesion area's *IoU* value of DS²Net_T is 69.81% achieving close segmentation results (73.03%) of OTU_CEUS-trained SegFormer (Tab.VI).

4) Ablation Study: To separately prove the efficiency of each module of DS²Net, we conduct experiments adapting OTU_2d to OTU_CEUS. From Tab. VIII, we analyze in the following points. (1) Compared to PSPNet without domain

TABLE VIII

ABLATION EXPERIMENTS ADAPTING OTU_2d TO OTU_CEUS.
“SYMMETRIC” DENOTES THE SYMMETRIC ARCHITECTURE WITH DUAL ENCODERS AND DECODER-HEADS, I.E. DS²NET REMOVING D_{E_s} , D_{E_t} , DDSM AND DUSM (FIG.6). “+” MEANS APPENDING.

Methods	\mathcal{L}_{seg}^{ss}	\mathcal{L}_{seg}^{st}	$\mathcal{L}_{adv}^{E_s}$	$\mathcal{L}_{adv}^{E_t}$	<i>IoU</i> (%)	<i>mIoU</i> (%)
PSPNet (w/o DA)	-	-	-	-	50.57	67.87
+ Symmetric (w/o DA)	✓	✓	-	-	50.88	67.93
+ Feature alignment (FA)	✓	✓	✓	✓	57.08	72.55
+ DDSM	✓	✓	✓	✓	59.28	74.53
+ DUSM (DS ² Net_P)	✓	✓	✓	✓	61.85	75.75
SegFormer (w/o DA)	-	-	-	-	61.11	75.45
+ Symmetric (w/o DA)	✓	✓	-	-	61.01	75.33
+ Feature alignment (FA)	✓	✓	✓	✓	64.74	77.54
+ DDSM	✓	✓	✓	✓	68.06	79.78
+ DUSM (DS ² Net_T)	✓	✓	✓	✓	69.81	80.86

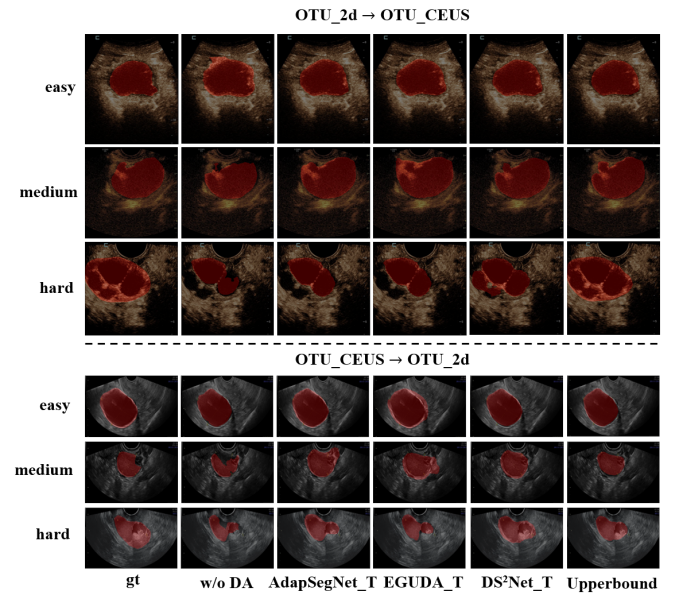


Fig. 9. Visualization comparison between different methods. We select segformer-based models as example. “Upperbound” indicates the results from single-modality training model.

adaptation, only applying symmetric structure can not bring improvement, because domain shift problem still exists. (2) When adding feature alignment mechanism, the performance significantly improve. This reflects that feature alignment makes effect on alleviating the domain shift problem and improves the general representation capability of E_s and E_t . (3) When appending DDSM, the architecture further improves. The reason is that DDSM guides the optimization trend making the target images become easier to be represented into target-style. (4) When appending DUSM, the architecture still achieves improvement benefiting from universal feature extraction.

5) Visualization and Analysis: To intuitively show the performance of DS²Net, we compare the segmentation performance of different methods. The qualitative results are shown in Fig.9. We can see that only training model without domain

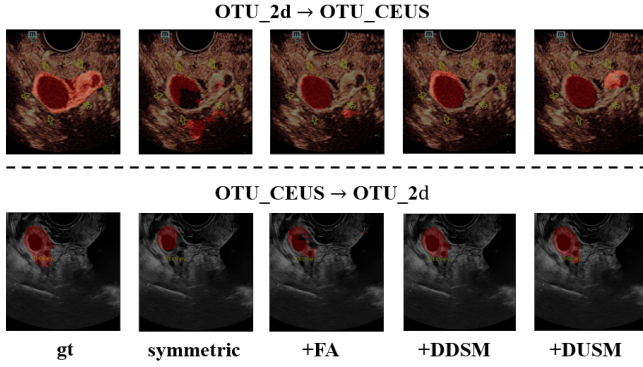


Fig. 10. Visualization comparison to illustrate the effectiveness of each module. We select segformer-based models as example.

TABLE IX

SINGLE-MODALITY RECOGNITION RESULTS ON MMOTU IMAGE DATASET. WE ADOPT TOP1 AND TOP2 ACCURACY AS OUR METRIC.

Methods	OTU_2d		OTU_CEUS	
	top1 (%)	top2 (%)	top1 (%)	top2 (%)
ResNet-34	77.61	88.70	69.0	79.0
ResNet-50	80.17	90.19	72.0	81.0
DenseNet-121	78.89	89.34	69.0	77.0
EfficientNet-b0	76.12	85.93	64.0	79.0
EfficientNet-b1	77.61	86.99	71.0	79.0

adaptation can work well on some easy cases, but can not handle harder cases. Benefiting from feature alignment mechanism, AdapSegNet and EGUDA can generate reasonable predictions under most cases, even on hard cases. Obviously, DS²Net shows the most powerful performance. On medium and hard cases, DS²Net can capture more semantic information and achieve most close results to “Upperbound”.

To directly show the effectiveness of each module, we also conduct visualization analysis. As shown in Fig.10, symmetric architecture does not work well, because dual encoders and decoder-heads can not solve domain shift problems. When applying feature alignment mechanism, the model can generate reasonable predictions. When appending DDSM, the model can generate more semantically reasonable predictions. When adding DUSM, the final DS²Net shows the strongest representation capability. This visualization comparison coincides with the ablation experiments shown in Tab.VIII, which further makes DS²Net more convincing and interpretable.

C. Single-Modality Recognition Results

On Task1 and Task2, we apply a “foreground-background” lesion area segmentation without directly applying seven/eight-category segmentation. Therefore, we tackle single-modality image recognition in Task3 (Fig.1) to classify ovarian tumors. In this paper, we provide ResNet, DenseNet and EfficientNet as baseline classification models. For all models, we select SGD as optimizer. The momentum and weight decay value are set as 0.9 and 0.0005. All model

are loaded ImageNet-pretrained weights before training. As shown in Tab.IX, we find that ResNet-50 outperforms other methods. EfficientNet-b1 achieves close results to ResNet-50 on OTU_CEUS, which shows better generalization capability training with less samples. Moreover, besides top1 accuracy, we also use top2 accuracy as metric because providing two category candidates is also valuable for diagnosis in practical medical treatment.

VI. CONCLUSION

In this paper, we propose a multi-modality ovarian tumor ultrasound (MMOTU) image dataset to explore the cross-domain representation potential. MMOTU image dataset contains 1469 2d ultrasound images and 170 CEUS images with pixel-wise and global-wise annotations. Based on MMOTU image dataset, we mainly focus on alleviating the domain shift problems on lesion area segmentation for bidirectional unsupervised domain adaptation between 2d ultrasound and CEUS images. In this paper, we propose DS²Net, which is a feature alignment based architecture. Specifically, we use adversarial learning to first ease the domain shift of encoders for better representation capability on both source and target images. Then, we design DDSM and DUSM to extract the domain-distinct and domain universal features. With these two modules, each encoder and decoder-head will further have specific style feature representation capability towards both source and target images. Extensive experiments show that the DS²Net outperforms the previous notable feature alignment based methods on MMOTU image dataset. Visualization and analysis also prove that DS²Net is convincing and interpretable. In this paper, we also provide series of baseline models on single-modality semantic segmentation and recognition tasks. Compared to previous methods, we first propose method to tackle the cross-domain ovarian tumor segmentation on our proposed MMOTU image dataset, which provides a new insight on detecting ovarian tumors. In the future, we will further extend our work and focus on the following aspects. (1) We will continually extend our proposed MMOTU image dataset, especially OTU_CEUS. We will also pay attention to preserving pure data without symbols. (2) Actually, the total tumor categories of OTU_2d are 32. Since some of tumor types (e.g. fibrosarcoma) have only one or two samples, we exclude them in our dataset. In the future, we will extend the categories together with collecting more data. (3) In MMOTU image dataset, samples of each category are unbalanced. We will further explore its influence. (4) In this work, we explore the AI-aided techniques on CEUS images. Based on this research, we will further explore the AI-aided methods on CEUS sequences, which will be more valuable and meaningful.

APPENDIX

As mentioned in Fig.3, there are some symbols on images, where some of them are just marked on the lesion area. Due to some historical and practical reason, we can not collect pure data without symbols. Naturally, there may raise a question, is there a risk of biasing the model by symbols

TABLE X

SEMANTIC SEGMENTATION RESULTS COMPARISON BETWEEN MODELS TRAINED BY IMAGES WITH AND W/O SYMBOLS. ON SINGLE-MODALITY SEGMENTATION, WE SELECT PSPNET AND SEGFORMER AS EXAMPLE.

Single-modality segmentation results on MMOTU image dataset				
Methods	OTU_2d		OTU_CEUS	
	<i>IoU</i> (%)	<i>mIoU</i> (%)	<i>IoU</i> (%)	<i>mIoU</i> (%)
PSPNet	82.01	89.41	71.01	81.6
PSPNet (w/o symbols)	81.13	88.63	70.78	81.09
SegFormer	82.46	89.88	73.03	83.0
SegFormer (w/o symbols)	81.52	89.17	72.62	82.55

UDA segmentation results on MMOTU image dataset				
Methods	OTU_CEUS → OTU_2d		OTU_2d → OTU_CEUS	
	<i>IoU</i> (%)	<i>mIoU</i> (%)	<i>IoU</i> (%)	<i>mIoU</i> (%)
DS ² Net_P	54.06	71.87	61.85	75.75
DS ² Net_P (w/o symbols)	52.93	70.46	60.49	74.62
DS ² Net_T	65.42	79.2	69.81	80.86
DS ² Net_T (w/o symbols)	64.03	78.02	68.58	79.43

during optimization? In this section, we conduct experiments on single-modality 2d ultrasound image segmentation and cross-domain segmentation tasks to analyze the influence of symbols.

To remove the symbols from images, we apply the recent notable image inpainting method [47] on all samples in MMOTU image dataset. Then we use the original and “symbol-free” MMOTU image dataset to respectively train models. We will discuss the results shown in Tab.X as follows. (1) Generally, models trained with “symbol-free” samples show performance decline. (2) This comparison is a little bit unreasonable because the training and testing set both changes after removing the symbols. However, we can still roughly draw a conclusion that applying image inpainting technique is not necessary. (3) Intuitively, images after removing symbols are not becoming distorted or destroyed. However, it also change the data in an implicit manner. (4) From another perspective, experts are not confused by those symbols during annotating the images, which means the symbols have little impact on visual features of images. Therefore, we believe that our models can also learn those important and useful features.

REFERENCES

- [1] R. L. Siegel, K. D. Miller, H. E. Fuchs *et al.*, “Cancer statistics, 2021,” *CA: A Cancer Journal for Clinicians*, vol. 71, no. 1, 2021.
- [2] C. Wu, Y. Wang, and F. Wang, “Deep learning for ovarian tumor classification with ultrasound images,” in *Advances in Multimedia Information Processing PCM*, ser. Lecture Notes in Computer Science, vol. 11166, 2018, pp. 395–406.
- [3] Y. Wang and Q. Zeng, “Ovarian tumor texture classification based on sparse auto-encoder network combined with multi-feature fusion and random forest in ultrasound image,” *J. Medical Imaging Health Informatics*, vol. 11, no. 2, pp. 424–431, 2021.
- [4] X. Yang, H. Li, Y. Wang *et al.*, “Contrastive rendering with semi-supervised learning for ovary and follicle segmentation from 3d ultrasound,” *Medical Image Anal.*, vol. 73, p. 102134, 2021.
- [5] J. Qian, R. Li, X. Yang *et al.*, “HASA: hybrid architecture search with aggregation strategy for echinococcosis classification and ovary segmentation in ultrasound images,” *CoRR*, vol. abs/2204.06697, 2022.
- [6] H. Li, J. Fang, S. Liu *et al.*, “Cr-unet: A composite network for ovary and follicle segmentation in ultrasound images,” *IEEE J. Biomed. Health Informatics*, vol. 24, no. 4, pp. 974–983, 2020.
- [7] Y. Tsai, W. Hung, S. Schulter *et al.*, “Learning to adapt structured output space for semantic segmentation,” in *IEEE Conference on Computer Vision and Pattern Recognition*, 2018, pp. 7472–7481.
- [8] J. Hoffman, E. Tzeng, T. Park *et al.*, “Cycada: Cycle-consistent adversarial domain adaptation,” in *International Conference on Machine Learning*, vol. 80, 2018, pp. 1994–2003.
- [9] J. Zhu, T. Park, P. Isola *et al.*, “Unpaired image-to-image translation using cycle-consistent adversarial networks,” in *IEEE International Conference on Computer Vision*, 2017, pp. 2242–2251.
- [10] C. Chen, Q. Dou, H. Chen *et al.*, “Unsupervised bidirectional cross-modality adaptation via deeply synergistic image and feature alignment for medical image segmentation,” *IEEE Trans. Medical Imaging*, vol. 39, no. 7, pp. 2494–2505, 2020.
- [11] D. Zou, Q. Zhu, and P. Yan, “Unsupervised domain adaptation with dual-scheme fusion network for medical image segmentation,” in *International Joint Conference on Artificial Intelligence*, 2020, pp. 3291–3298.
- [12] J. Chi, E. Walia, P. S. Babyn *et al.*, “Thyroid nodule classification in ultrasound images by fine-tuning deep convolutional neural network,” *J. Digit. Imaging*, vol. 30, no. 4, pp. 477–486, 2017.
- [13] H. Wang, C. Liu, Z. Zhao *et al.*, “Application of deep convolutional neural networks for discriminating benign, borderline, and malignant serous ovarian tumors from ultrasound images,” *Frontiers in Oncology*, vol. 11, 2021.
- [14] Y. Zhang, H. Chen, Y. Wei *et al.*, “From whole slide imaging to microscopy: Deep microscopy adaptation network for histopathology cancer image classification,” in *Medical Image Computing and Computer Assisted Intervention*, vol. 11764, 2019, pp. 360–368.
- [15] M. Zhu, Z. Chen, and Y. Yuan, “Dsi-net: Deep synergistic interaction network for joint classification and segmentation with endoscope images,” *IEEE Trans. Medical Imaging*, vol. 40, no. 12, pp. 3315–3325, 2021.
- [16] X. He, Y. Deng, L. Fang, and Q. Peng, “Multi-modal retinal image classification with modality-specific attention network,” *IEEE Trans. Medical Imaging*, vol. 40, no. 6, pp. 1591–1602, 2021.
- [17] O. Ronneberger, P. Fischer, and T. Brox, “U-net: Convolutional networks for biomedical image segmentation,” in *Medical Image Computing and Computer-Assisted Intervention*, vol. 9351, 2015, pp. 234–241.
- [18] J. Chen, Y. Lu, Q. Yu *et al.*, “Transunet: Transformers make strong encoders for medical image segmentation,” *CoRR*, vol. abs/2102.04306, 2021. [Online]. Available: <https://arxiv.org/abs/2102.04306>
- [19] Z. Zhou, M. M. R. Siddiquee, N. Tajbakhsh, and J. Liang, “Unet++: A nested u-net architecture for medical image segmentation,” in *Deep Learning in Medical Image Analysis - and - Multimodal Learning for Clinical Decision Support*, vol. 11045, 2018, pp. 3–11.
- [20] Y. Zhang, H. Liu, and Q. Hu, “Transfuse: Fusing transformers and cnns for medical image segmentation,” in *Medical Image Computing and Computer Assisted Intervention*, vol. 12901, 2021, pp. 14–24.
- [21] C. Ouyang, K. Kamnitsas, C. Biffi *et al.*, “Data efficient unsupervised domain adaptation for cross-modality image segmentation,” in *Medical Image Computing and Computer Assisted Intervention*, vol. 11765, 2019, pp. 669–677.
- [22] G. Zeng, T. D. Lerch, F. Schmaranzer *et al.*, “Semantic consistent unsupervised domain adaptation for cross-modality medical image segmentation,” in *Medical Image Computing and Computer Assisted Intervention*, vol. 12903, 2021, pp. 201–210.
- [23] L. Du, J. Tan, H. Yang *et al.*, “SSF-DAN: separated semantic feature based domain adaptation network for semantic segmentation,” in *IEEE International Conference on Computer Vision*, 2019, pp. 982–991.
- [24] S. Wang, L. Yu, X. Yang *et al.*, “Patch-based output space adversarial learning for joint optic disc and cup segmentation,” *IEEE Trans. Medical Imaging*, vol. 38, no. 11, pp. 2485–2495, 2019.
- [25] G. Zeng, F. Schmaranzer, T. D. Lerch *et al.*, “Entropy guided unsupervised domain adaptation for cross-center hip cartilage segmentation from MRI,” in *Medical Image Computing and Computer Assisted Intervention*, vol. 12261, 2020, pp. 447–456.
- [26] D. S. Wanderley, C. B. Carvalho, A. Domingues *et al.*, “End-to-end ovarian structures segmentation,” in *Progress in Pattern Recognition, Image Analysis, Computer Vision and Applications*, vol. 11401, 2018, pp. 681–689.
- [27] P. Mathur, K. Kakwani, Diplav *et al.*, “Deep learning based quantification of ovary and follicles using 3d transvaginal ultrasound in assisted reproduction,” in *International Conference of the Engineering in Medicine & Biology Society*, 2020, pp. 2109–2112.
- [28] O. Oktay, J. Schlemper, L. L. Folgoc *et al.*, “Attention u-net: Learning where to look for the pancreas,” *CoRR*, vol. abs/1804.03999, 2018.

- [29] X. Chen, R. Zhang, and P. Yan, “Feature fusion encoder decoder network for automatic liver lesion segmentation,” in *International Symposium on Biomedical Imaging*, 2019, pp. 430–433.
- [30] C. Kaul, S. Manandhar, and N. E. Pears, “Focusnet: An attention-based fully convolutional network for medical image segmentation,” in *International Symposium on Biomedical Imaging*, 2019, pp. 455–458.
- [31] M. Paschali, S. Gasperini *et al.*, “3dq: Compact quantized neural networks for volumetric whole brain segmentation,” in *Medical Image Computing and Computer Assisted Intervention*, vol. 11766, 2019, pp. 438–446.
- [32] Z. Wang, N. Zou, D. Shen *et al.*, “Non-local u-nets for biomedical image segmentation,” in *AAAI Conference on Artificial Intelligence*, 2020, pp. 6315–6322.
- [33] A. Dosovitskiy, L. Beyer, A. Kolesnikov *et al.*, “An image is worth 16x16 words: Transformers for image recognition at scale,” in *International Conference on Learning Representations*, 2021.
- [34] H. Cao, Y. Wang, J. Chen *et al.*, “Swin-unet: Unet-like pure transformer for medical image segmentation,” *CoRR*, vol. abs/2105.05537, 2021.
- [35] Z. Liu, Y. Lin, Y. Cao *et al.*, “Swin transformer: Hierarchical vision transformer using shifted windows,” in *IEEE International Conference on Computer Vision*, 2021, pp. 9992–10 002.
- [36] S. Li, X. Sui, X. Luo *et al.*, “Medical image segmentation using squeeze-and-expansion transformers,” in *International Joint Conference on Artificial Intelligence*, 2021, pp. 807–815.
- [37] P. Isola, J. Zhu, T. Zhou *et al.*, “Image-to-image translation with conditional adversarial networks,” in *IEEE Conference on Computer Vision and Pattern Recognition*, 2017, pp. 5967–5976.
- [38] R. T. Narra, N. Singhal, N. S. Narayan *et al.*, “Automated ovarian volume quantification in transvaginal ultrasound,” in *International Symposium on Biomedical Imaging*, 2018, pp. 1513–1516.
- [39] H. Zhao, J. Shi, X. Qi *et al.*, “Pyramid scene parsing network,” in *IEEE Conference on Computer Vision and Pattern Recognition*, 2017, pp. 6230–6239.
- [40] J. Fu, J. Liu, H. Tian *et al.*, “Dual attention network for scene segmentation,” in *IEEE Conference on Computer Vision and Pattern Recognition*, 2019, pp. 3146–3154.
- [41] E. Xie, W. Wang, Z. Yu *et al.*, “Segformer: Simple and efficient design for semantic segmentation with transformers,” in *Advances in Neural Information Processing Systems*, vol. 34, 2021, pp. 12 077–12 090.
- [42] C. Yu, C. Gao, J. Wang *et al.*, “Bisenet V2: bilateral network with guided aggregation for real-time semantic segmentation,” *Int. J. Comput. Vis.*, vol. 129, no. 11, pp. 3051–3068, 2021.
- [43] K. He, X. Zhang, S. Ren, and J. Sun, “Deep residual learning for image recognition,” in *IEEE Conference on Computer Vision and Pattern Recognition*, 2016, pp. 770–778.
- [44] G. Huang, Z. Liu, L. van der Maaten *et al.*, “Densely connected convolutional networks,” in *IEEE Conference on Computer Vision and Pattern Recognition*, 2017, pp. 2261–2269.
- [45] M. Tan and Q. V. Le, “Efficientnet: Rethinking model scaling for convolutional neural networks,” in *International Conference on Machine Learning*, vol. 97, 2019, pp. 6105–6114.
- [46] J. Deng, W. Dong, R. Socher *et al.*, “Imagenet: A large-scale hierarchical image database,” in *IEEE Conference on Computer Vision and Pattern Recognition*, 2009, pp. 248–255.
- [47] J. Yu, Z. Lin, J. Yang *et al.*, “Free-form image inpainting with gated convolution,” in *IEEE International Conference on Computer Vision*, 2019, pp. 4471–4480.